CCFE
CULHAM CENTRE FOR FUSION ENERGY

UK Atomic Energy Authority

UKAEA-CCFE-PR(20)121

Guoliang Xia, Yueqiang Liu, L. Li, C. J. Ham, Z . Wang, Shuo Wang

Effects of poloidal and parallel flows on resistive wall mode instability in toroidally rotating plasmas

Effects of poloidal and parallel flows on resistive wall mode instability in toroidally rotating plasmas

Guoliang Xia, Yueqiang Liu, L. Li, C. J. Ham, Z . Wang, Shuo Wang

This is a preprint of a paper submitted for publication in Nuclear Fusion Letter

Effects of poloidal and parallel flows on resistive wall mode instability in toroidally rotating plasmas

Guoliang Xia[1,2], Yueqiang Liu[3], L. Li[4,5], C.J. Ham[1], Z.R. Wang[6], Shuo Wang[2]

[1]CCFE, Culham Science Centre, Abingdon, OX14 3DB, United Kingdom of Great Britain and Northern Ireland
[2]Southwestern Institute of Physics, PO Box 432, Chengdu 610041, People's Republic of China
[3]General Atomics, PO Box 85608, San Diego, CA 92186-5608, United States of America
[4]College of Science, Donghua University, Shanghai 201620, People's Republic of China
[5]Member of Magnetic Confinement Fusion Research Centre, Ministry of Education, People's Republic of China
[6]Princeton Plasma Physics Laboratory, Princeton, NJ 08543, United States of America

E-mails of corresponding authors Guoliang.Xia@ukaea.uk, liuy@fusion.gat.com

Abstract

Effects of parallel and poloidal flows, as well as the flow shear, on the resistive wall mode (RWM) instability have been numerically investigated in toroidally rotating plasmas, utilizing a recently updated version of the MARS-F code (Liu Y Q *et al* 2000 Phys. Plasmas **7** 3681). A significant difference between these flows is that the background toroidal flow frequency is symmetric with respect to the poloidal angle, whilst both the poloidal and toroidal projections of the additional parallel flow are functions of both the plasma minor radius and poloidal angle. It is found that the stability of the resistive wall mode is hardly modified by the parallel flow, as a consequence of cancellation of the stabilizing effect provided by the poloidal projection of the parallel flow from one side, and the destabilizing effect provided by the toroidal projection from the other side. The destabilizing effect of the toroidal projection comes predominantly from the m=1 poloidal Fourier harmonic of the flow contribution. The shear of the parallel flow is found to generally weaken the

stabilization/destabilization effect on the RWM, as compared to the case of uniform parallel flow.

1. Introduction

The resistive wall mode (RWM) can limit the operational space of advanced tokamaks, which aim at producing high pressure, large faction of bootstrap current, long-pulse or steady state plasmas. Since advanced tokamak scenarios are envisaged for most of the future devices such as HL-2M [1], JT-60SA [2], ITER [3] as well as CFETR [4], understanding the RWM stabilization physics, under various plasma conditions, is still an important and urgent task, despite extensive efforts that have been taken during recent years in studying this plasma instability.

The RWM can be viewed as a residual instability from the external ideal kink (XK) mode [5], which is a low-*n* (*n* is the toroidal mode number), global magneto-hydrodynamic (MHD) instability driven by plasma current and/or pressure. For a pressure driven XK, the normalized plasma pressure, the $\beta_N = \beta(\%)\, a(m)\, B_0(T) / I_p(MA)$ value controls the mode stability, where β is the ratio of the volume averaged plasma pressure to the magnetic pressure, I_p the total plasma current, *a* the plasma minor radius, and B_0 the vacuum toroidal magnetic field. When β_N exceeds a critical value (the so-called Troyon no-wall limit [6]), the XK becomes unstable. A close-fitting perfectly conducting wall can stabilize the XK, resulting in (often substantially) increased β_N. However, the presence of a resistive wall (often a vacuum vessel of the tokamak) only reduces the XK growth rate without

shifting the stability boundary, converting the XK to a RWM growing on a timescale characteristic of the field penetration time through the wall. A truly unstable RWM can hardly non-linearly saturate due to the global nature of the instability, thus often leading to major disruptions of the plasma, causing the so-called hard beta limit. It is thus highly desirable to achieve the RWM stabilization, in order to maximize the economic benefit for advanced tokamaks.

It is now well established that either active control [7-12] or plasma toroidal flow in combination with drift kinetic effects [13-19], or the synergistic actions from both [20-22], can potentially stabilize the RWM. Active control is based on magnetic coils to compensate the field perturbation which passes through the resistive wall. Magnetic feedback experiments, carried out in both tokamaks [23, 24] and reversed field pinches [25, 26], as well as extensive theoretical investigations [9, 27], have demonstrated that successful suppression of the RWM can increase the plasma beta up to the ideal wall beta limit. On the other hand, passive stabilization of the mode, relying on the plasma flow and drift kinetic effects, appears more attractive (without using magnetic coils and sensors) if this can offer a full suppression of the RWM. This is also the subject of the present study.

Within the MHD description, the RWM stabilization mainly comes from the ion sound wave damping and the shear Alfven wave continuum damping [13-15, 28, 29]. The critical toroidal rotation velocity, required for complete stabilization of the mode, is normally a few percent of the Alfven speed [30]. On the other hand, MHD-kinetic hybrid theory, including drift kinetic resonances [18, 19, 31-33], predicts substantially

lower value (even down to zero) of the critical toroidal rotation speed required for the mode stabilization, thus offering a better explanation of recent experimental results obtained in DIII-D [34] and JT-60U [35].

So far, most of previous work on passive stabilization of the RWM only assumes toroidal plasma flow, neglecting any effects from the poloidal and/or parallel flow of the plasma. This is partially due to the fact that the poloidal flow is usually strongly damped in a tokamak device due to neoclassical effects [36]. On the other hand, recent experiments in JET have shown that the poloidal flow velocity of the plasma can be one order of magnitude higher than the neoclassical prediction [37, 38]. This often occurs in discharges where internal transport barrier (ITB) has been observed. In fact, a strong poloidal flow appears to be an important player in forming ITB.

In this work, we investigate the n=1 RWM stabilization by various combinations of the poloidal and toroidal flows. By doing so, we clarify the fundamental physics associated with the (general) flow damping of the RWM. This study thus further advances the previous understanding achieved in [39], where the poloidal flow is found to play an important role on the RWM stabilization, due to coupling to the toroidal flow via the parallel flow.

The next section discusses the computational model with parallel/poloidal flow. A toroidal equilibrium, assumed in thus study, is also briefly described here. Section 3 reports numerical results. Section 4 concludes the work.

2. Computational model and equilibrium model

2.1. Toroidal MHD model with parallel/poloidal flow in MARS-F code

In this work, the MHD stability code MARS-F [7] is updated to include a generic equilibrium flow, i.e. both toroidal and poloidal flows. MARS-F employs a curve-linear flux coordinate system (s, χ, ϕ), where the radial coordinate $s = \sqrt{\psi_N}$ (ψ_N is the normalized equilibrium poloidal flux, being equal to 0 at the magnetic axis and unity at the plasma boundary) labels the magnetic flux surface, χ a generic poloidal angle and ϕ the geometric toroidal angle. The equilibrium magnetic field is represented as

$$\mathbf{B} = \nabla\phi \times \nabla\psi + T(\psi)\nabla\phi,$$

where ψ is the equilibrium poloidal magnetic flux [note that ψ here is not normalized to 0 and 1], T is the poloidal current flux function.

Within the single fluid model, an equilibrium flow satisfying mass conservation can be generally represented as

$$\mathbf{V}_0 = R^2 \left[\Omega_t(s) + \hat{\Omega}(s, \chi) \right] \nabla\phi + \rho^{-1} U(s) \mathbf{B}, \quad (1)$$

where R is the plasma major radius, $\Omega_t(s) + \hat{\Omega}(s, \chi)$ the angular velocity of a generic toroidal flow of the plasma, $U(s)$ the flow component parallel to the equilibrium magnetic field lines, and ρ the equilibrium plasma density normalized to unity at the magnetic axis. In this work, we consider sub-sonic equilibrium flow. Therefore, the plasma flow induced modification to the equilibrium is neglected.

Note that we introduce a generic toroidal flow component $\hat{\Omega}(s, \chi)$ in our model (1), that varies along both the plasma minor radius and poloidal angle [40]. This

makes our flow model different from that assumed in [39]. This does not contradict the mass conservation law $\nabla\bullet(\rho\mathbf{V}_0)=0$. However, assumption of additional physics constraint, such as the radial ion force balance, will eliminate the $\hat{\Omega}(s,\chi)$ component, in which case the 1-D component $\Omega_t(s)$ represents the sum of the toroidal $\mathbf{E}\times\mathbf{B}$ and the ion diamagnetic rotation frequencies. Nevertheless, in this study, we shall keep the 2-D component $\hat{\Omega}(s,\chi)$ in our equilibrium flow model. As we will see later, this allows us to study the effect of a pure poloidal flow on the MHD instability.

The parallel flow component $U(s)$ is always a 1-D function, in order to satisfy equilibrium mass conservation. The parallel flow can be projected into the toroidal and poloidal directions, resulting in

$$\begin{cases}\Omega_\phi(s,\chi)=\Omega_t(s)+\hat{\Omega}(s,\chi)+\rho^{-1}U(s)\dfrac{T}{R^2},\\ \Omega_\chi(s,\chi)=\rho^{-1}U(s)\dfrac{\psi'}{J},\end{cases} \tag{2}$$

where J is the Jacobian associated with the curve-linear coordinates (s,χ,ϕ). A choice of $\hat{\Omega}(s,\chi)=-\rho^{-1}U(s)T/R^2$ and $\Omega_t(s)=0$ leaves us with a pure poloidal equilibrium flow. On the other hand, setting $\hat{\Omega}(s,\chi)=0$ as well as $\Omega_t(s)=0$ allows us to study the effect of pure equilibrium parallel flow on the MHD instability. Finally, setting $U(s)=0$ and $\hat{\Omega}(s,\chi)=0$, the conventional case of a pure 1-D toroidal flow is recovered.

Inclusion of parallel/poloidal flow leads to additional terms (underlined below) to the perturbed MHD equations, as compared to the previous formulation [7, 13, 14] with toroidal flow alone

$$\rho_1 = -\nabla\bullet(\rho\xi), \tag{3}$$

$$\begin{aligned}(\gamma + in\Omega)\xi = {} & \mathbf{v} + (\xi\bullet\nabla\Omega)R^2\nabla\phi \\ & \underline{-\rho^{-1}U\nabla\times(\xi\times\mathbf{B}) + \rho^{-2}U\rho_1\mathbf{B} + (\xi\bullet\nabla U)\rho^{-1}\mathbf{B}},\end{aligned} \tag{4}$$

$$\begin{aligned}\rho(\gamma + in\Omega)\mathbf{v} = {} & -\nabla p + \mathbf{j}\times\mathbf{B} + \mathbf{J}\times\mathbf{b} - \rho[2\Omega\hat{\mathbf{Z}}\times\mathbf{v} + (\mathbf{v}\bullet\nabla\Omega)R^2\nabla\phi] \\ & - \rho\kappa_{\|}|k_{\|}|v_{th,i}[\mathbf{v}\bullet\hat{\mathbf{b}} + \underline{(\xi\bullet\nabla\mathbf{V}_0)\bullet\hat{\mathbf{b}}}]\hat{\mathbf{b}} \\ & \underline{-U\nabla(\mathbf{v}\bullet\mathbf{B}) + U\mathbf{v}\times\mathbf{J} + U\mathbf{B}\times(\nabla\times\mathbf{v}) - \mathbf{B}[\rho\nabla(\rho^{-1}U)\bullet\mathbf{v}]},\end{aligned} \tag{5}$$

$$(\gamma + in\Omega)\mathbf{b} = \nabla\times(\mathbf{v}\times\mathbf{B}) + (\mathbf{b}\bullet\nabla\Omega)R^2\nabla\phi\underline{-\nabla\times(\rho^{-1}U\mathbf{b}\times\mathbf{B})}, \tag{6}$$

$$p = -\xi\bullet\nabla P - \Gamma P\nabla\bullet\xi, \tag{7}$$

$$\mu_0\mathbf{j} = \nabla\times\mathbf{b}, \tag{8}$$

where γ is the (generally complex) eigenvalue of the instability, corrected by a Doppler shift $in\Omega$ with $\Omega = \Omega_t(s) + \hat{\Omega}(s,\chi)$. The quantities $(\rho_1, \boldsymbol{\xi}, \mathbf{v}, \mathbf{b}, \mathbf{j}, p)$ represent the plasma perturbed density, displacement, velocity, magnetic field, current and pressure, respectively. The symbols $(\rho, \mathbf{B}, \mathbf{J}, P)$ are equilibrium quantities, obtained by the equilibrium code CHEASE [41]. $\hat{\mathbf{Z}}$ is the unit vector in the vertical direction, $\kappa_{\|}$ the strength of the parallel sound wave damping, $k_{\|} = (n - m/q)/R$ the parallel wave number, with *m* being the poloidal harmonic number and *q* the safety factor. $v_{th,i} = \sqrt{2T_i/M_i}$ is the thermal ion velocity, with T_i , M_i being the thermal ion temperature and mass. $\hat{\mathbf{b}} = \mathbf{B}/B$ is the unit vector along the equilibrium magnetic field. Γ is the ratio of specific heats, taken to be 5/3 for an ideal gas.

In the vacuum region, the perturbed magnetic field satisfies divergence-free conditions. In the region occupied by the resistive wall, an eddy current equation is solved following a thin shell approximation [20]. The above new formulation (1)-(8) has been implemented into the MARS-F code. A series of tests have been carried out

to verify the new code.

2.2. Equilibrium model

We consider an up-down symmetric equilibrium, with the plasma boundary shape shown in figure 1(a). The shape of the resistive wall conforms to the plasma boundary surface. The key equilibrium radial profiles are plotted in Fig. 1(b-e). Note that we choose a slightly reversed magnetic shear in the plasma core, which is often compatible with the advanced tokamak scenario in the presence of ITB [42]. The safety factor has the on-axis value of $q_0 = 1.76$, the minimal value of $q_{\min} = 1.6$, and the edge value of $q_e = 3.28$. The normalized beta value for this equilibrium is $\beta_N = 3.37$. The no-wall beta limit is computed as $\beta_N^{no-wall} = 2.54$, and the beta limit with an ideal wall is $\beta_N^{ideal-wall} = 3.72$. A linear scaling factor for the equilibrium pressure, C_β, is consequently introduced $C_\beta = (\beta_N - \beta_N^{no-wall})/(\beta_N^{ideal-wall} - \beta_N^{no-wall})$, yielding $C_\beta = 0.52$ for the equilibrium shown in Fig. 1.

The radial profiles for the plasma toroidal rotation frequency $\Omega_t(s)$ (solid line) and the parallel flow component $U(s)$ (dashed line), are shown in Fig. 2. The $\Omega_t(s)$ profile is chosen from an early JET discharge [43], and $U(s)$ is a scaled-down version of $\Omega_t(s)$. Note that in this work, the toroidal rotation frequency is normalized by the on-axis toroidal Alfven frequency $\Omega_A = B_0/(R_0\sqrt{\mu_0\rho_0})$, and the parallel component U is normalized by $U_N = R_0\Omega_A/B_0$. Whilst the amplitude of these plasma flow speeds will be scanned in our study, we generally assume that the poloidal flow is slower than the toroidal

flow. This is a reasonable assumption taking considering neoclassical poloidal flow damping.

3. Numerical results

In the following four sub-sections, with the new MARS-F implementation, we shall investigate the n=1 RWM instability affected by (i) parallel flow, (ii) a pure poloidal flow, (iii) toroidal projection of parallel flow and (iv) flow shear, respectively. In these computations, we do not consider full drift kinetic effects on the RWM stability, but instead include a simpler viscous type of model involving ion-Landau damping of parallel sound waves.

3.1. Effect of parallel flow on RWM stability

The effect of parallel flow on the RWM has previously been considered in Ref. 39. The results there imply that parallel flow has a strong effect on the mode stability. A close analysis of the modeling procedure in Ref. 39 reveals that the authors assume that the total toroidal flow, including that of the toroidal projection of the parallel flow, is fixed while introducing the parallel flow. This means that, when the parallel flow is introduced, Ref. 39 also changes the toroidal flow component $\Omega_t(s)$ in Eq. (2) from Section 2.1 above, such that the total toroidal flow $\Omega_\phi(s,\chi)$ from Eq. (2) is approximately fixed (assuming $\hat{\Omega}(s,\chi)=0$). Note that the total toroidal flow cannot be exactly fixed, since the toroidal projection of the parallel flow is a 2-D flow, which cannot be exactly replaced by the 1-D flow $\Omega_t(s)$. Certain proxy has to be taken, e.g.

by taking the toroidal projection of the parallel flow only along the outboard mid-plane.

We have followed the same procedure in our study, and find qualitatively similar results to Ref. 39. In what follows, however, we choose another approach, in order to more clearly identify the role of parallel flow on the RWM stability. This, together with results to be shown in the follow-up section (Section 3.2), clarifies the RWM damping physics, when both the parallel/poloidal and toroidal plasma flows are present.

More specifically, we shall keep the toroidal flow component $\Omega_t(s)$ fixed while scanning the parallel flow velocity. For comparison, we first report MARS-F results in the absence of parallel flow (Fig. 3). In this case, a strong parallel sound wave damping, in combination with the Alfven and sound wave continua resonances, fully stabilizes the RWM at sufficiently fast toroidal flow. The critical rotation frequency, required for complete stabilization of the mode, is $\Omega_{cri} = 0.045$. This result is expected following the fluid theory for the RWM [13].

Next, we fix the toroidal rotation $\Omega_t(s)$ and vary the parallel flow component $U(s)$ ($\hat{\Omega}(s,\chi)$ is set to zero). The shapes of the radial profiles for $\Omega_t(s)$ and $U(s)$ are taken from Fig. 2. The on-axis values for $\Omega_t(s)$ are fixed at $\Omega_0 = 0.02$ and $\Omega_0 = 0.04$, respectively. The latter flow amplitude is close to the critical value for the RWM stabilization as found from Fig. 3. The MARS-F results, reported in Fig. 4, show that the stability of the RWM is hardly modified by the parallel flow.

As for an intuitive understanding, a plasma flow along the equilibrium field line

mainly introduces a rotational transform. In other words, the MHD physics remains the same if a reference frame were introduced which flowed along the field lines. This transform is not trivial to perform though in practice. Another intuitive interpretation is that the RWM dynamics, like many other macroscopic MHD instabilities, involve mainly physics along the perpendicular (to field lines) direction. (This is not strictly true though, since we know that the parallel dynamics couple to the perpendicular motion through the plasma compressibility.) When the plasma is close to be incompressible (which holds at the marginal stability point for ideal MHD), and the additional coupling via sub-sonic equilibrium flow (due to centrifugal and Coriolis forces) is weak, the parallel dynamics is not important.

Figure 5 further demonstrates that the effect of parallel flow is very weak on the RWM stability. The stability window [14], in terms of the wall minor radius, is found to undergo little modification, when the parallel flow is introduced in either positive (to the equilibrium parallel current) or negative directions. This holds for both toroidal rotation cases considered here.

3.2. Effect of poloidal flow on RWM stability

As discussed in Section 2.1, the parallel flow can be projected into poloidal and toroidal components. In this sub-section, we study the effect of a pure poloidal flow on the RWM stability. The toroidal projection of the parallel flow is eliminated for these simulations by setting $\hat{\Omega}(s,\chi) = -\rho^{-1}U(s)T/R^2$ in Eq. (2).

Here, we present numerical results showing stabilization of the RWM by the

pure poloidal flow in a toroidally rotating plasma. We again keep the toroidal flow fixed while scanning the parallel flow speed U. Figure 6 shows two examples of the computed RWM eigenvalue versus the on-axis value of U, fixing the toroidal rotation frequency at $\Omega_0 = 0.02$ (circles) and $\Omega_0 = 0.04$ (squares), respectively. We emphasize that only the poloidal projection of the parallel flow is included in these computations.

It is apparent that the growth rate of the RWM decreases with increasing U_0, although U_0 is much smaller than the toroidal rotation frequency. The mode becomes stable for both cases, when U_0 the exceeds a critical value of $U_0 = 1.5\times10^{-3}$. The stabilizing effect of the pure poloidal flow is found to be stronger for the case with slower background toroidal flow. In fact, the mode growth rate decreases about five times quicker (with increasing U_0) for the plasma rotating at $\Omega_0 = 0.02$, than the case of $\Omega_0 = 0.04$, as shown in Fig. 6(a).

Figure 7 further demonstrates the substantial effect of poloidal flow on the RWM stability. The width of the stability window increases with (positive) U_0, when the poloidal projection alone is included in the computations, as shown in Fig. 7(a). With negative U_0, addition of poloidal flow destabilizes the RWM and narrows the stability window.

3.3. Effect of toroidal projection of parallel flow on RWM stability

Now we consider the opposite case, where we only keep the toroidal projection of parallel flow. Note that this flow component varies along both the plasma minor

radius as well as the poloidal angle, unlike the 1-D toroidal flow $\Omega_t(s)$ which is also included here.

Figure 8 reports the U_0-scan results at fixed 1-D flow $\Omega_t(s)$, with all the parameters being the same as Fig. 6, except replacing the poloidal projection by the toroidal projection. We again find that the larger effect from the U_0-scan occurs at slower toroidal rotation $\Omega_0 = 0.02$. The critical value for marginal stability, in terms of U_0, is similar between two values of Ω_0.

What is counter-intuitive is that increasing U_0 *destabilizes* the RWM, despite the fact that the toroidal projection of parallel flow and the 1-D toroidal flow $\Omega_t(s)$ have the same sign when U_0 is positive. In order to understand this effect, we decompose the toroidal projection into poloidal Fourier harmonics $\hat{\Omega}(s,\chi) = \rho^{-1}U(s)T/R^2 = \Omega_{m=0}(s) + 2Re[\sum_{m=1}\Omega_m(s)e^{im\chi}]$. The dominant harmonics turn out to be *m*=0 and *m*=1 (and -1). These are shown in Fig. 9(a). The *m*=0 harmonic has the same (positive) sign as $\Omega_t(s)$. The *m*=1 (or -1) harmonic, however, has the opposite sign. The computed destabilization, shown by Fig. 8, comes from the Fourier harmonic coupling effect with the *m*=1 component of the 2-D flow $\hat{\Omega}(s,\chi)$, as demonstrated by Fig. 9(b).

Indeed, by including the *m*=0 component of $\hat{\Omega}(s,\chi)$ alone, Fig. 9(b) shows stabilizing effect, as expected. On the other hand, a strong destabilization occurs if we only include the *m*=1 component of $\hat{\Omega}(s,\chi)$ into the MARS-F computation. Note that this destabilization must come from toroidal coupling effect, not simply due to the fact that the *m*=1 harmonic has opposite sign to the 1-D flow $\Omega_t(s)$. This is

because the flow associated with the *m*=1 component changes direction along the poloidal angle. The surface averaged contribution to the flow, from the *m*=1 component, thus vanishes.

3.4. Effect of flow shear on RWM stability

In what follows, we investigate how the change of flow shear for the parallel flow component $U(s)$ affects the RWM stability. We introduce a set of parallel flow profiles, $U = U_0(1-s^{\mu})^{\nu}$, with different choices of (μ,ν) -values. Three representative choices are shown in Fig. 10. Note that case 1 (uniform profile with vanishing shear) and case 3 (strong local shear near the *q*=2 surface) represent two extreme situations.

The MARS-F computed RWM eigenvalues, assuming the above three profiles for the parallel flow $U(s)$, are reported in Fig. 11. Note that, besides the flow shear variation, we also compare cases with inclusion of poloidal or toroidal projection alone of the parallel flow, or with inclusion of the full parallel flow. In the latter, the flow shear of $U(s)$ has negligible effect on the RWM stability, largely due to the fact that the parallel flow itself has a very weak effect on the mode. On the other hand, the flow shear associated with the poloidal or toroidal projection significantly affects the mode stability. Generally the effect is weaker with stronger shear. It is important to note that this conclusion holds if we fix the parallel flow amplitude at the *q*=2 surface ($U_{q=2}$) while varying the shear. Although generally there is no unique way of comparison, we find out that this is the best way to isolate the flow shear effect from

that of the flow amplitude.

Compared to the case without parallel flow or its projections (i.e. $U_{q=2}=0$), stabilization or destabilization of the RWM depends on the direction of the parallel flow. Stabilization of the mode is achieved either by poloidal projection of parallel flow in the positive direction (aligning with the equilibrium parallel current), or by toroidal projection of parallel flow in the negative direction. Destabilization is found in opposite cases.

4. Conclusions and discussion

We carried out detailed numerical investigation on the *n*=1 RWM stabilization by various combination of the poloidal/parallel and toroidal plasma flows, utilizing the updated version of MARS-F code. The effect of the flow shear of the parallel flow has also been studied.

One of the key findings is that the parallel flow provides minor stabilization to the RWM. At a first glance, this may be contradicting to the conclusion reached by Aiba et al. [39]. In their work, the parallel flow was introduced with fixed total amount of toroidal flow. In our work, we fix the 1-D toroidal flow frequency while adding the parallel flow component. This allows to study the effect of a pure parallel flow on the mode stability. Our result suggests that the parallel flow acts more like introducing a rotational transform (along the equilibrium field line) to the mode, than providing physical stabilization.

On the other hand, if we keep only the poloidal or toroidal component of the

parallel flow, the effect on the RWM stability is appreciable, even at small magnitude of parallel flow, i.e. at about 10% of that of the 1-D background toroidal flow speed. With the same sign for the 1-D toroidal flow and the parallel flow, we find that the poloidal projection of the parallel flow provides additional stabilization to the RWM, whilst the toroidal projection destabilizes the mode. As a result, when both the poloidal and toroidal components are included (i.e. with full parallel flow), the stabilization and destabilization effects cancel each other, resulting in a minor effect of parallel flow on the RWM stability.

An interesting observation is that, despite the fact that the toroidal projection of parallel flow in average enhances the 1-D background toroidal flow, the RWM stability is reduced. We find out that this destabilization originates from the m=1 poloidal Fourier harmonic of the toroidal projection, which has an opposite sign to the 1-D background flow. This m=1 component destabilizes the mode via mode coupling effect.

The shear of the parallel flow component, near the q=2 surface, generally weakens the effect on the RWM stabilization/destabilization. Consequently, a large shear at the q=2 rational surface with negative poloidal projection or positive toroidal projection reduces the mode destabilization. A uniform parallel flow with positive poloidal projection or negative toroidal projection enhances the mode stabilization.

The finding that a small amount of poloidal flow can effect appreciable stabilization to the RWM may be important for ITER, where the toroidal flow is not expected to be fast, and the drift kinetic stabilization (at slow toroidal flow) is

predicted to only partially stabilize the mode [31].

The aforementioned drift kinetic effects have been ignored in this study, for the purpose of reaching clear physics understanding within the fluid picture. Combination of parallel flow, or its poloidal/toroidal projections, with drift kinetic theory requires further development of the MHD-kinetic hybrid formulation. In particular, the particle bounce orbit average of the toroidal projection (which is a function of both plasma minor radius and poloidal angle) of the parallel flow need to be added into the drift kinetic resonance operators. The resonance between poloidal flow and particle drift motions has so far not been considered in the kinetic RWM theory, although the physics is similar to that of the magnetic pumping for the neoclassical poloidal flow damping. Detailed hybrid formulation still need to be developed, which will be part of a future work.

Acknowledgments

This work is supported by NSFC with Grant No. 11605046, 11705050, 11805054, 11847219, NMCFSP with Grant No. 2015GB105001, the National Key R&D Program of China under contract No. 2017YFE0301100, 2017YFE0301104 and the Royal Society K. C. Wong International Fellowship. The work is also supported by U.S. DoE Office of Science under Contract Nos. DE-FG02–95ER54309 and DE-FC02–04ER54698. The project is also partly funded by the RCUK Energy Programme [grant number EP/P012450/1]. To obtain further information on the data and models underlying this paper please contact PublicationsManager@ukaea.uk.

Guoliang Xia would like to thank Dr Samuli Saarelma for helpful suggestions.

References

[1] Li Q 2015 *Fusion Eng. Des.* **96-97** 338-342

[2] Mastrostefano S, Bettini P, Bolzonella T, Palumbo M F, Liu Y, Matsunaga G, Specogna R, Takechi M, Villone F 2015 *Fusion Eng. Des.* **96** 659-663

[3] Hender T C *et al* 2007 *Nucl. Fusion* **47** S128-S202

[4] Wan B, Ding S, Qian J, Li G, Xiao B, Xu G 2014 *IEEE Transactions on Plasma Science* **42** 495-502

[5] Chu M S, Okabayashi M 2010 *Plasma Phys. Control. Fusion* **52** 123001

[6] Troyon F, Gruber R, Saurenmann H, Semenzato S, Succi S 1984 *Plasma Phys. Control. Fusion* **26** 209-215

[7] Liu Y Q, Bondeson A, Fransson C M, Lennartson B, Breitholtz C 2000 *Phys. Plasmas* **7** 3681

[8] Fransson C M, Lennartson B, Breitholtz C, Bondeson A, Liu Y Q 2000 *Phys. Plasmas* **7** 4143

[9] Okabayashi M *et al* 2001 *Phys. Plasmas* **8** 2071

[10] Liu Y Q, Bondeson A, Gribov Y, Polevoi A 2004 *Nucl. Fusion* **44** 232-242

[11] Strait E J *et al* 2004 *Phys. Plasmas* **11** 2505

[12] Bondeson A, Liu Y Q, Fransson C M, Lennartson B, Breitholtz C, Taylor T S 2001 *Nucl. Fusion* **41** 455

[13] Bondeson A, Ward D 1994 *Phys. Rev. Lett.* **72** 2709

[14] Chu M S, Greene J M, Jensen T H, Miller R L, Bondeson A, Johnson R W, Mauel M E 1995 *Phys. Plasmas* **2** 2236

[15] Betti R, Freidberg J P 1995 *Phys. Rev. Lett.* **74** 2949

[16] Strait E J, Taylor T, Turnbull A, Ferron J, Lao L, Rice B, Sauter O, Thompson S, Wróblewski D 1995 *Phys. Rev. Lett.* **74** 2483

[17] Liu Y Q, Chu M S, Chapman I T, Hender T C 2008 *Phys. Plasmas* **15** 112503

[18] Hu B, Betti R 2004 *Phys. Rev. Lett.* **93** 105002

[19] Berkery J W, Sabbagh S A, Reimerdes H, Betti R, Hu B, Bell R E, Gerhardt S P, Manickam J, Podestà M 2010 *Phys. Plasmas* **17** 082504

[20] Xia G, Liu Y, Liu Y Q 2014 *Plasma Phys. Control. Fusion* **56** 095009

[21] Xia G, Liu Y Q, Liu Y, Hao G, Li L 2015 *Nucl. Fusion* **55** 093007

[22] Chu M S *et al* 2004 *Phys. Plasmas* **11** 2497

[23] Okabayashi M *et al* 2005 *Nucl. Fusion* **45** 1715-1731

[24] Sabbagh S, Bell R, Menard J, Gates D, Sontag A, Bialek J, LeBlanc B, Levinton F, Tritz K, Yuh H 2006 *Phys. Rev. Lett.* **97** 045004

[25] Drake J R *et al* 2005 *Nucl. Fusion* **45** 557-564

[26] Martin P *et al* 2009 *Nucl. Fusion* **49** 104019

[27] Bialek J, Boozer A H, Mauel M E, Navratil G A 2001 *Phys. Plasmas* **8** 2170

[28] Gregoratto D, Bondeson A, Chu M S, Garofalo A M 2001 *Plasma Phys. Control. Fusion* **43** 1425-1439

[29] Zheng L J, Kotschenreuther M, Chu M 2005 *Phys. Rev. Lett.* **95** 255003

[30] Ward D J, Bondeson A 1995 *Phys. Plasmas* **2** 1570
[31] Liu Y Q *et al* 2009 *Phys. Plasmas* **16** 056113
[32] Zheng L J, Kotschenreuther M T, Van Dam J W 2009 *Nucl. Fusion* **49** 075021
[33] Liu Y Q *et al* 2010 *Plasma Phys. Control. Fusion* **52** 104002
[34] Reimerdes H *et al* 2007 *Phys. Rev. Lett.* **98** 055001
[35] Takechi M, Matsunaga G, Aiba N, Fujita T, Ozeki T, Koide Y, Sakamoto Y, Kurita G, Isayama A, Kamada Y 2007 *Phys. Rev. Lett.* **98** 055002
[36] Doyle E J *et al* 2007 *Nucl. Fusion* **47** S18-S127
[37] Crombe K *et al* 2005 *Phys. Rev. Lett.* **95** 155003
[38] Tala T *et al* 2007 *Nucl. Fusion* **47** 1012-1023
[39] Aiba N, Shiraishi J, Tokuda S 2011 *Phys. Plasmas* **18** 022503
[40] Li L, Liu Y Q, Loarte A, Schmitz O, Liang Y, Zhong F C 2018 *Phys. Plasmas* **25** 082512
[41] Lütjens H, Bondeson A, Sauter O 1996 *Comput. Phys. Commun.* **97** 219
[42] Bondeson A, Liu D H, Söldner F X, Persson M, Baranov Y F, Huysmans G T A 1999 *Nucl. Fusion* **39** 1523
[43] Liu Y Q, Saarelma S, Gryaznevich M P, Hender T C, Howell D F 2010 *Plasma Phys. Control. Fusion* **52** 045011

Figures and figure captions

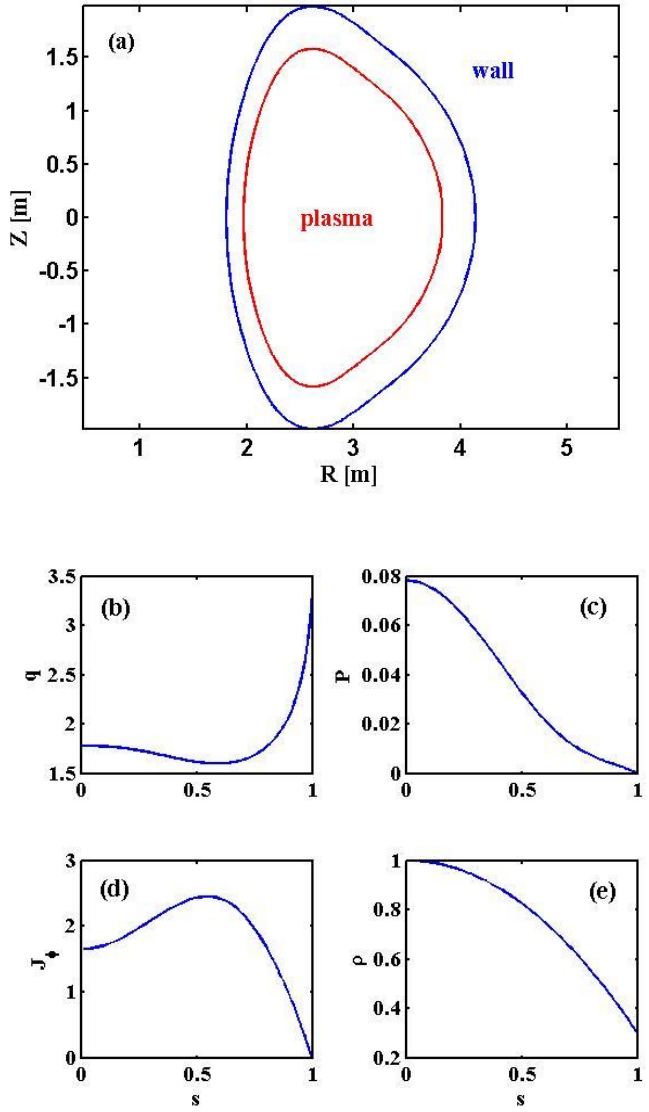

Figure 1. (a) Geometry of an up-down symmetric equilibrium shown in the poloidal cross section. With a JET-like plasma shape and a conformal resistive wall. Shown also are equilibrium radial profiles for (b) the safety factor, (c) the plasma pressure normalized by B_0^2/μ_0, (d) the surface averaged toroidal current density normalized by $B_0/(\mu_0 R_0)$, and (e) the plasma density normalized to unity at the magnetic axis. Here $s=\sqrt{\psi_N}$ labels the plasma minor radius, with ψ_N being the normalized poloidal equilibrium magnetic flux.

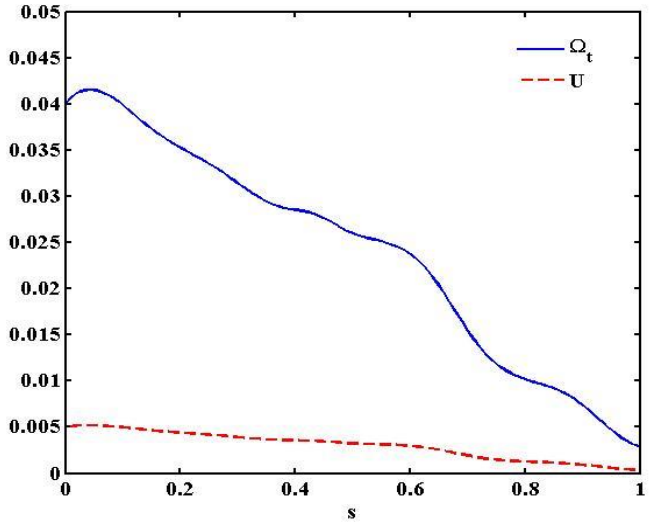

Figure 2. The radial profiles for the plasma toroidal rotation frequency (solid line), normalized by $\Omega_A = B_0 / (R_0 \sqrt{\mu_0 \rho_0})$ and the plasma parallel flow component (dashed line), normalized by $U_N = R_0 \Omega_A / B_0$.

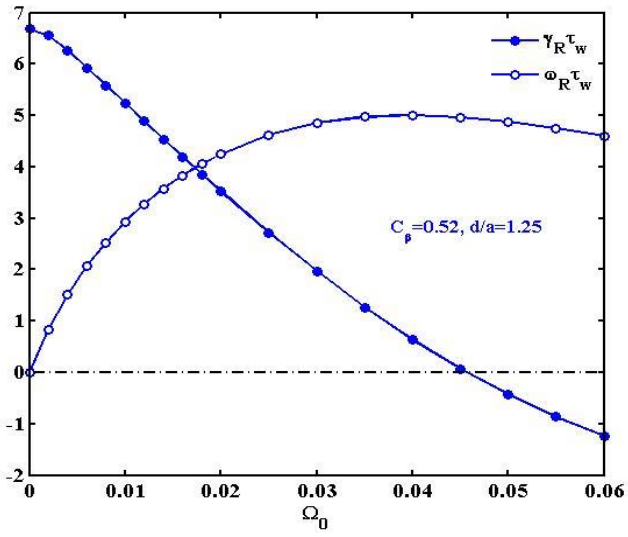

Figure 3. Growth rate (γ_R) and mode frequency (ω_R) of the *n*=1 RWM versus the plasma on-axis toroidal rotation frequency. The other parameters are fixed: the plasma pressure $C_\beta = 0.52$, the normalized wall distance $d/a = 1.25$ and the parallel viscous damping coefficient $\kappa_{\|} = 1.5$.

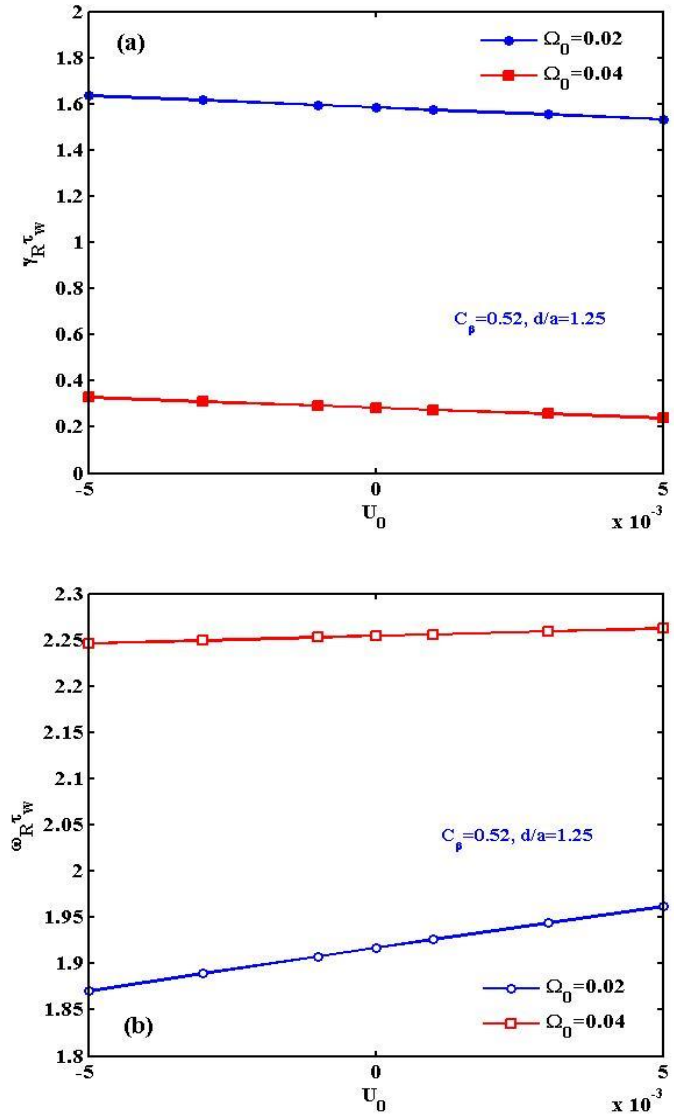

Figure 4. (a) Growth rate and (b) mode frequency of the RWM versus the plasma on-axis parallel flow component for two choices of the toroidal rotation at the plasma centre $\Omega_0 = 0.02$ (circles) and $\Omega_0 = 0.04$ (squares), respectively. The other parameters are fixed: $C_\beta = 0.52$, $d/a = 1.25$ and $\kappa_{||} = 1.5$. The toroidal rotation frequency is normalized by the on-axis toroidal Alfven frequency $\Omega_A = B_0 / (R_0 \sqrt{\mu_0 \rho_0})$, and the parallel flow component is normalized by $U_N = R_0 \Omega_A / B_0$.

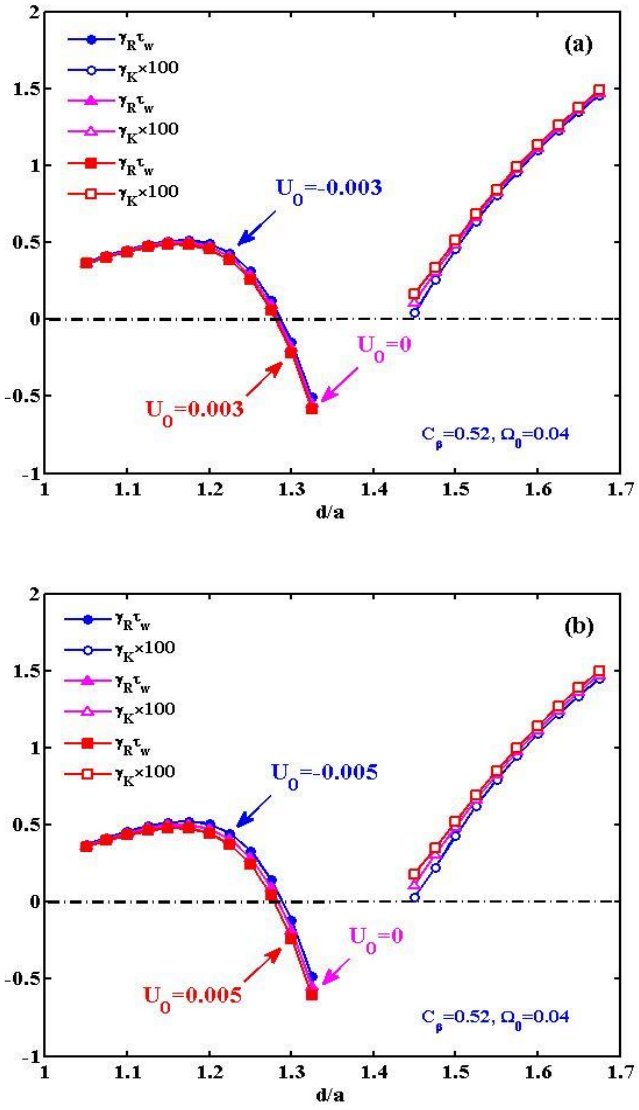

Figure 5. Growth rates of the RWM (γ_R) and the XK (γ_K) versus the normalized wall position for different choices of the parallel flow component, at the values of (a) $U_0 = 0.003$ and (b) $U_0 = 0.005$. The other parameters are fixed: the plasma pressure $C_\beta = 0.52$, the parallel viscous damping coefficient $\kappa_{||} = 1.5$ and the toroidal rotation frequency $\Omega_0 = 0.04$.

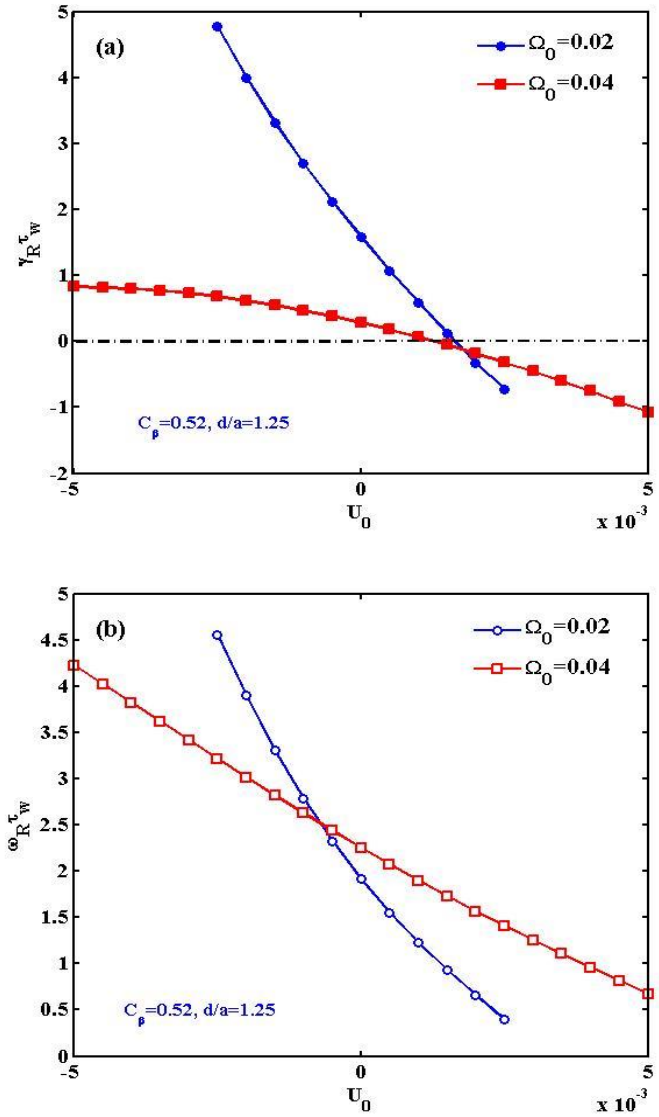

Figure 6. (a) Growth rate and (b) mode frequency of the RWM versus the plasma on-axis parallel flow speed for two choices of the toroidal rotation at the plasma centre $\Omega_0 = 0.02$ (circles) and $\Omega_0 = 0.04$ (squares), respectively. Only the poloidal projection of parallel flow is included while scanning U_0. The other parameters are fixed: the plasma pressure $C_\beta = 0.52$, the normalized wall distance $d/a = 1.25$ and the parallel viscous damping coefficient $\kappa_{||} = 1.5$. The toroidal rotation frequency is normalized by the on-axis toroidal Alfven frequency $\Omega_A = B_0 / (R_0 \sqrt{\mu_0 \rho_0})$, and the parallel flow component is normalized by $U_N = R_0 \Omega_A / B_0$.

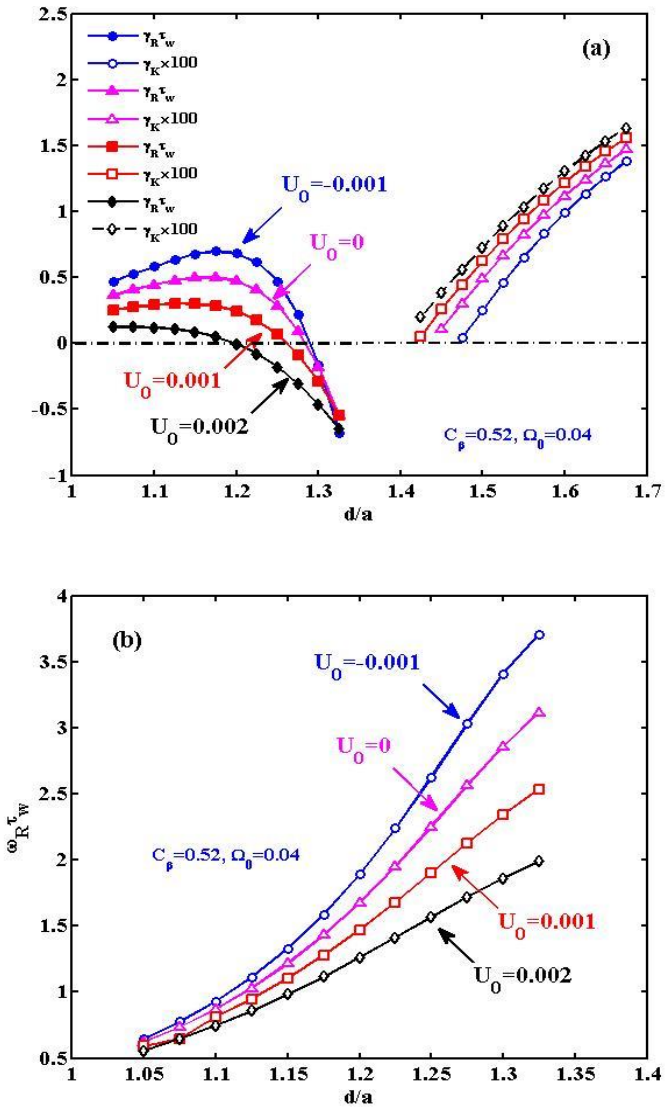

Figure 7. (a) Growth rates of the RWM (γ_R) and the XK (γ_K), and (b) mode frequency of the RWM versus the normalized wall radius, for different choices of the on-axis parallel flow speed at $U_0 = -0.001$ (circles), $U_0 = 0$ (triangles), $U_0 = 0.001$ (squares) and $U_0 = 0.002$ (diamonds). Only the poloidal projection of parallel flow is included while scanning U_0. The other parameters are fixed: the plasma pressure $C_\beta = 0.52$, the parallel viscous damping coefficient $\kappa_{||} = 1.5$ and the toroidal rotation frequency $\Omega_0 = 0.04$.

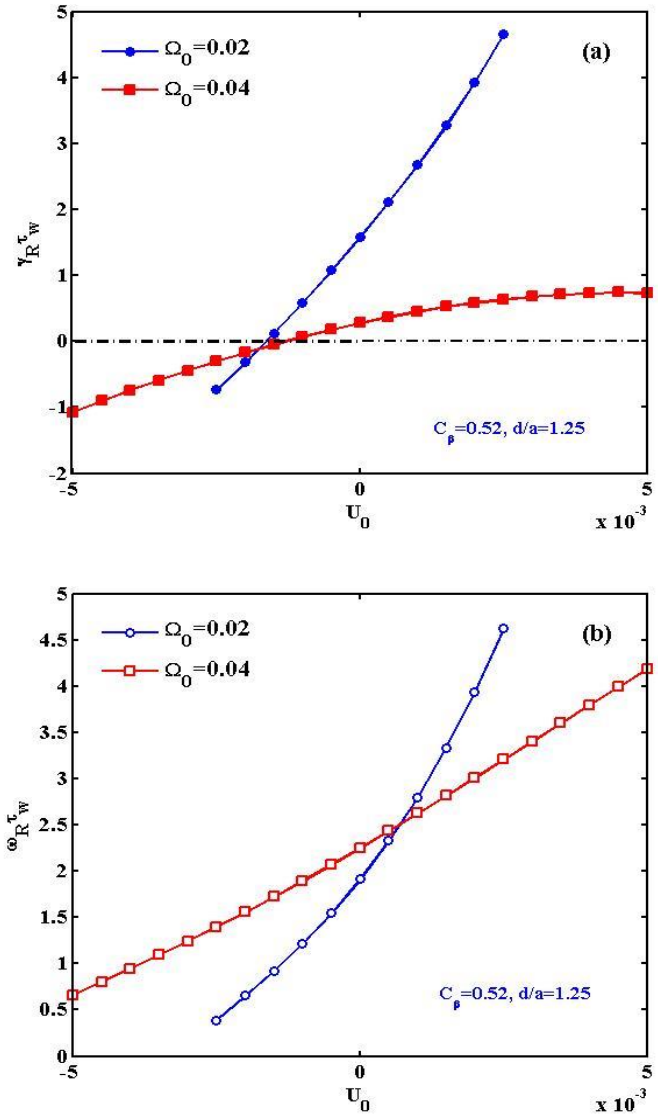

Figure 8. (a) Growth rate and (b) mode frequency of the RWM versus the plasma on-axis parallel flow component for two choices of the toroidal rotation at the plasma center $\Omega_0 = 0.02$ (circles) and $\Omega_0 = 0.04$ (squares), respectively. Only the toroidal projection of parallel flow is included while scanning U_0. The other parameters are fixed: $C_\beta = 0.52$, $d/a = 1.25$ and $\kappa_{||} = 1.5$. The toroidal rotation frequency is normalized by the on-axis toroidal Alfven frequency $\Omega_A = B_0 \big/ (R_0 \sqrt{\mu_0 \rho_0})$, and the parallel flow component is normalized by $U_N = R_0 \Omega_A / B_0$.

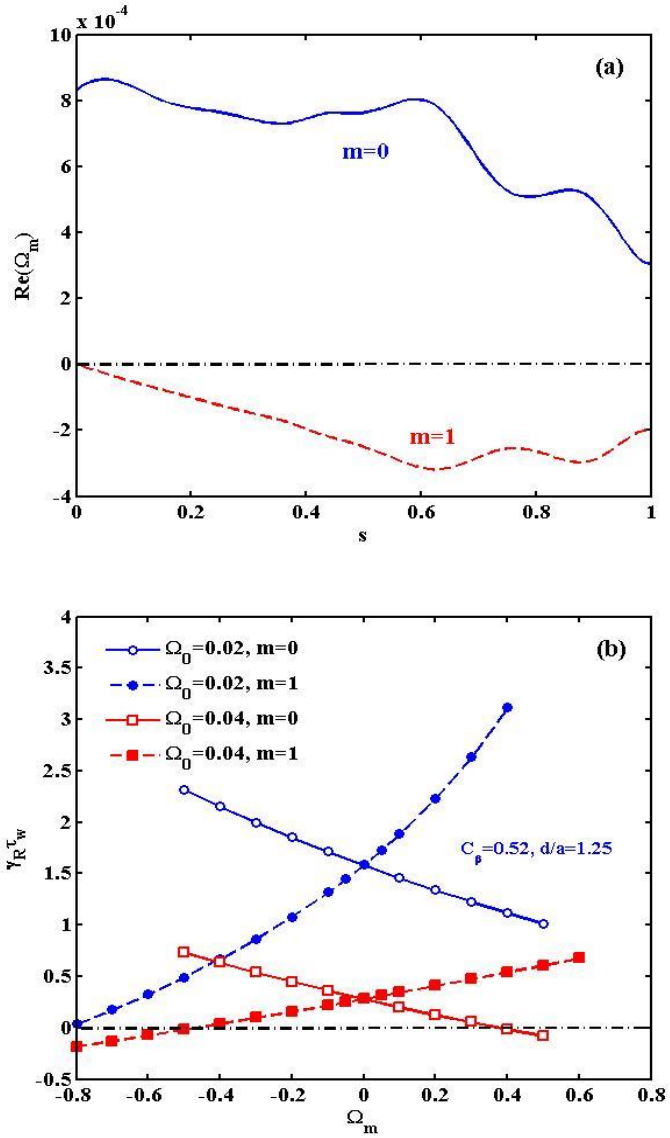

Figure 9. (a) Radial profiles for the real parts of toroidal projection, with poloidal harmonics of *m*=0 and *m*=1, the other harmonics are at least 10 times smaller than the *m*=1 by amplitude and the imaginary parts of all harmonics are very small, (b) growth rate of the RWM versus the amplitude of each harmonic (*m*=0 and *m*=1) for two choices of the toroidal rotation $\Omega_0 = 0.02$ (circles) and $\Omega_0 = 0.04$ (squares), respectively. Note that the *m*=0 component is included into toroidal flow $\Omega_t(s)$.

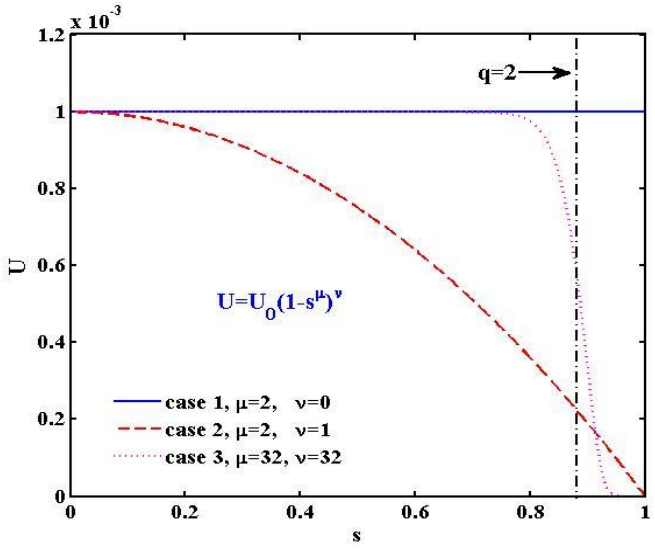

Figure 10. Three choices of the radial profile for the parallel flow component: uniform (case 1, solid), parabolic (case 2, dashed) and with a large local shear (case 3, dotted). The dash-dotted line denotes the location of the q=2 rational surface.

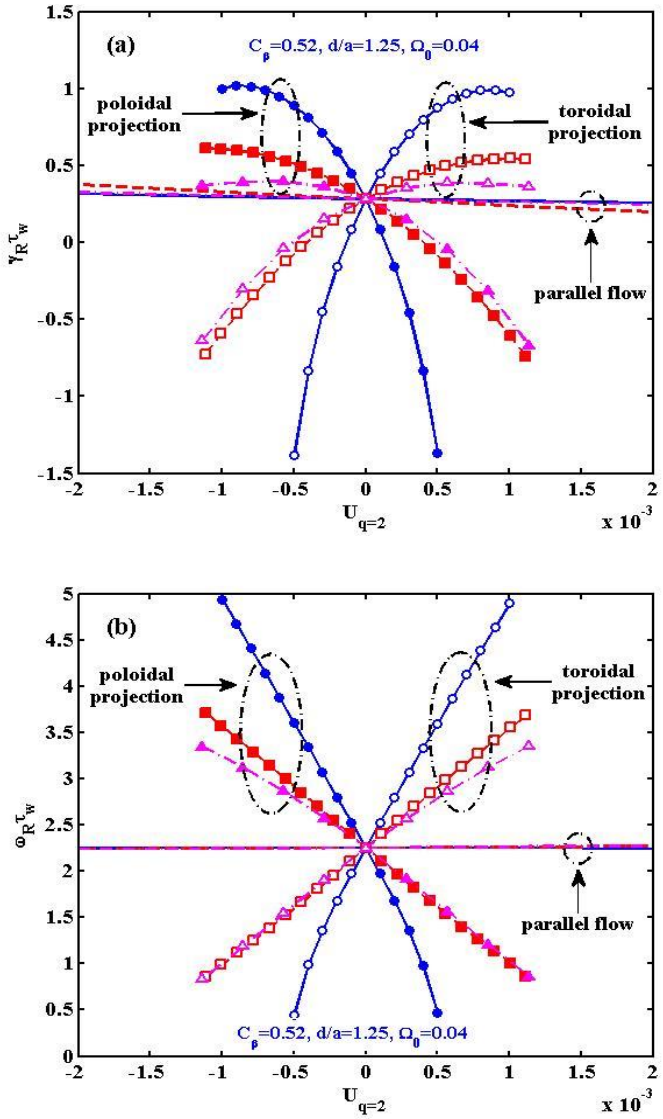

Figure 11. (a) Growth rate and (b) mode frequency of the RWM versus the parallel flow component at the *q*=2 rational surface, assuming three radial profiles as shown in Fig. 10: case 1 (uniform profile, circles), case 2 (parabolic profile, squares) and case 3 (large local shear, triangles). Compared are also three flow models: parallel flow (lines without symbols), only poloidal projection (filled symbols) and only toroidal projection (open symbols) component of parallel flow. Note that three curves with parallel flow are very close to each other. The other parameters are fixed: $C_\beta = 0.52$, $d/a = 1.25$, $\kappa_{||} = 1.5$ and $\Omega_0 = 0.04$.